European Polymer Journal 59 (2014) 262–269

Contents lists available at ScienceDirect

European Polymer Journal

journal homepage: www.elsevier.com/locate/europolj

Macromolecular Nanotechnology

Network formation of graphene oxide in poly (3-hydroxybutyrate) nanocomposites

Carlos R. Arza, Patric Jannasch, Frans H.J. Maurer *

Department of Chemistry, Polymer & Materials Chemistry, Lund University, P.O. Box 124, SE-22100 Lund, Sweden

ARTICLE INFO

Article history:
Received 27 May 2014
Received in revised form 24 July 2014
Accepted 28 July 2014
Available online 7 August 2014

Keywords:
PHB
Biopolymer
Graphene oxide
Shear modulus GO
Melt rheology
Network formation

ABSTRACT

Network formation of graphene oxide (GO) nanoplatelets was held accountable for the modification of the rheological properties of nanocomposites based on poly(3-hydroxybutyrate) (PHB). The nanocomposites were prepared by a casting procedure from the green solvent γ-butyrolactone. The nature of the GO network and percolation limits were analyzed by making use of the molar mass reduction of PHB that takes place in the melt, as well as by studying the deformation dependence of the viscoelastic behavior of the nanocomposites. The percolation volume fraction for the formation of GO network was found to be below 0.07%, while a corresponding GO aspect ratio of 400 was determined. The equilibrium shear modulus ($|G^*_{eq}|$) of the GO network and the critical strain γ_c of the nanocomposites could be described both by a power-law dependence on the volume fraction of GO nanoparticles. Further assessment of the structure formation of the GO nanoparticles was made in the solid state, wherein the shear modulus of GO was analyzed with the Halpin–Tsai model. The values thus determined suggested the existence of tiled nanoplatelets within the formed network structure in the nanocomposites. The thermal properties of the nanocomposites were examined by differential scanning calorimetry (DSC) and thermogravimetric analysis (TGA). The microstructure of the samples was also characterized using X-ray diffraction (XRD) measurements.

1. Introduction

Poly[(*R*)-3-hydroxybutyrate] (PHB) is a natural linear polyester that can be produced by a large number of microorganisms [1]. First discovered in 1926, it has since attracted much interest due to its biodegradability and production from renewable sources. Physical properties of PHB such as melting temperature, glass transition temperature, crystallinity, and tensile strength are comparable to those of commercial synthetic polymers [2]. However, PHB is not stable at processing temperatures above the melting temperature, and thermal degradation by chain scission with subsequent molar mass reduction is a serious issue [3–5]. Furthermore, PHB exhibits brittle fracture behavior at room temperature, and has a low strain at break of about 3%.

Modification of the physical properties of polymers can be achieved through the addition of nanofillers for the preparation of nanocomposites [6–8]. Polymer nanocomposites have been intensively studied during the last decade resulting in modified mechanical, electrical and gas barrier properties. Among the nanofillers studied, graphene-based materials have recently attracted most of the interest due to their two-dimensional (2D) nature, large theoretical specific surface area, and wide variety of physical and chemical properties [8]. A promising route for the mass production of this type of materials is by the modification and/or reduction of graphene oxide (GO) [9]. GO is typically obtained by oxidizing and exfoliating graphite

* Corresponding author. Tel.: +46 46 222 91 49.
E-mail address: Frans.Maurer@polymat.lth.se (F.H.J. Maurer).

http://dx.doi.org/10.1016/j.eurpolymj.2014.07.035
0014-3057/

in an appropriate solvent [10–12]. GO has also been used as a nanofiller for the preparation of nanocomposites based on i.e., chitosan [13], poly(methyl methacrylate) [14], poly(ethylene-2,6-naphthalate) [15], polyurethane [16], poly(lactic acid) [17], poly(ethylene terephthalate) [18], poly(butylene succinate) [19]. In all cases, the nanocomposites showed significant changes of some of their physical properties in relation to the properties of the neat polymer. The role of structure formation of the GO particles, however, as well as percolation limits are less often reported, and their role in structure property relations are not well understood.

The aim of the present study is to study the modification of the rheological properties of PHB by addition of GO nanoparticles and to contribute to the understanding of GO structure formation in PHB/GO nanocomposites. PHB/GO nanocomposites were prepared through a solvent casting procedure and the influence of GO on the melt rheology, thermal properties, solid state dynamic mechanical properties, and thermal degradation behavior of PHB was studied.

2. Materials and methods

2.1. Materials

Poly[(*R*)-3-hydroxybutyrate] (PHB) powder was supplied by BIOMER (Germany). The graphite used in this study was supplied by Asbury Graphite Mills (Expandable Graphite grade 3626). Hydrogen peroxide (35 wt% in water, Acros), potassium permanganate (98%, Acros), sulfuric acid (95–97%, Scharlab S.L.), hydrochloric acid (37 wt%, Honeywell), dimethyl sulfoxide (DMSO) (LABSCAN Analytical Sciences), and γ-butyrolactone (GBL) (99%, Sigma–Aldrich) were all used as received. The polymer was treated with 0.001 N aqueous HCl for 30 min and washed with deionized water three times. Finally, it was dried at 30 °C under vacuum for 5 days. The weight average molar mass (M_w) and the polydispersity index (PDI) after treatment was 620,000 g mol^{-1} and 2, respectively.

2.2. GO synthesis and sample preparation

Graphite oxide was synthesized from graphite by the modified Hummers method [20]. Sulfuric acid (260 mL) was mixed with graphite flakes (2 g) using a mechanical stirrer at 0 °C (ice bath) during 10 min. $KMnO_4$ (2 g) was added slowly and stirred at room temperature during 24 h. An additional, four $KMnO_4$ portions of 2 g each were added at a rate of one every 24 h. The reaction mixture was then quenched in 700 mL ice-water, and a 30% H_2O_2 solution (ca 10 mL) was added until it turned light-yellow. The mixture was centrifuged at 10,000 rpm for 20 min, and the colorless supernatant was decanted. The sediment was stirred for 30 min in 10% aqueous HCl solution (500 mL), and then centrifuged out at 10,000 rpm for 20 min. The separated graphite oxide was subsequently washed 3 times with deionized water (3 × 500 mL) by centrifuging at 10,000 rpm. Finally, the wet graphite oxide was dried at 30 °C under vacuum for 5 days. Dispersions of GO (2.5 mg mL^{-1}) were obtained by exfoliating graphite oxide in GBL under ultrasonic irradiation (Bransonic Ultrasonic Cleaner model 2510E-MTH) for 3 h. The dispersion was stored over molecular sieves (4 Å).

The nanocomposite films were prepared by solution casting from a 3 wt% polymer solution in GBL. The concentration of GO in the nanocomposites was kept in the range from 0.001 to 5 wt%. PHB powder was dissolved in GBL at 130 °C during 3 min. The solution was quickly cooled to 65 °C, followed by the addition of the required amount of GO dispersion at 65 °C. After stirring during 7 min, the dispersions were cast onto a petri dish and dried in an oven at 130 °C for 16 h. An additional series was prepared as described above with the exception of the PHB powder that was first dissolved in DMSO (final solvent ratio before casting was adjusted to GBL/DMSO = 62.5/37.5 v/v). For dynamic mechanical analysis in the solid state, samples were prepared between electrically heated platens (Graseby Specac) by compression molding the films at 180 °C for 2 min to produce samples with the dimensions 36 mm × 5 mm × 0.95 mm. Likewise, for dynamic mechanical analysis in the melt, samples were compression molded at 180 °C for 2 min into discs with a diameter of 15 mm and thickness of approx. 0.85 mm. Films pressed at 180 °C for 2 min were also used to collect the X-ray diffraction (XRD) patterns.

2.3. Characterization

XRD patterns were recorded with a Stoe Stadi MP Diffractometer in the reflection mode using Cu Kα radiation (0.145 nm).

Thermal transitions of the samples (ca 2 mg) were studied by differential scanning calorimetry (DSC, TA instruments Q2000). A first heating run from room temperature to 185 °C was performed to erase the thermal history of the material, followed by a cooling run to −70 °C, where both the enthalpy and temperature of crystallization were obtained. The glass transition and melt temperatures were obtained in a second heating run from −70 °C to 200 °C. The heating/cooling rates were 10 °C min^{-1}. Thermal decomposition of the nanocomposites and graphite oxide was determined by thermogravimetric analysis (TGA, TA instruments Q500). The TGA analysis was performed in a single heating run from room temperature to 500 °C for polymer-containing samples, and to 900 °C for the graphite oxide (ca 2 mg for all samples) at a heating rate of 10 °C min^{-1}.

Dynamic mechanical analysis both in the solid and melt state was performed with an Advanced Rheometer AR2000 ETC from TA Instruments. Rheological characterization in the melt was performed using parallel plates with a diameter of 15 mm under nitrogen atmosphere. The primary rheological quantities phase angle δ and the dynamic shear modulus $|G^*|$ were simultaneously determined at 185 °C as a function of elapsed time t_e. The phase angle $\delta(t_e)$ and the dynamic shear modulus $|G^*(t_e)|$ of pure PHB and nanocomposites were monitored by performing "time sweeps" in

the linear viscoelastic region, at an angular frequency of 6.28 rad s^{-1} (1 Hz). Each test was started 2.5 min after the insertion of the disc into the rheometer at 185 °C. A "stress sweep" between 2 and 10,000 Pa at frequency 6.28 rad s^{-1} (1 Hz) was performed to find the critical strain γ_c for the linear viscoelastic region. γ_c was defined as the strain at which $|G^*(\gamma)|/|G_0^*(\gamma)|$ decreases to 0.9 where $|G_0^*(\gamma)|$ is the linear extrapolation of $|G^*(\gamma)|$ starting from small strains in a $\log|G^*| - \log\gamma$ plot. The dynamic shear modulus in the solid state was recorded at 30 °C in the linear viscoelastic region at strain amplitude of 0.2%, an angular frequency of 62.83 rad s^{-1} (10 Hz), and a static pre-tension of 1 N.

3. Results and discussion

3.1. X-ray diffraction spectroscopy

Fig. 1 shows the XRD patterns for graphite, graphite oxide, PHB, and the nanocomposites containing 1, 3 and 5 wt% GO. The diffractogram of graphite oxide shows a reflection at $2\theta = 10.9°$ whereas the (002) reflection for graphite is present at $2\theta = 26.6°$. The disappearance of the latter reflection indicates the oxidation of graphite, and the increase of the spacing between graphite oxide layers due to intercalation of oxygen-containing groups [21–23]. The diffractograms for the nanocomposites containing 1, 3 and 5 wt% of GO presented neither reflection belonging to graphite oxide nor new reflections when compared with the XDR pattern of PHB, thus showing no evidence of discernible restacking of GO at room temperature after the preparation of the nanocomposites. Fig. 1, on the other hand, also showed differences among the XDR patterns of PHB and nanocomposites, mainly in the relative intensities of the reflections at $2\theta = 16°$ and $2\theta = 17°$ due to the (011) and (110) planes, respectively, as well as the relative intensities of the three reflections between $2\theta = 20°$ and $2\theta = 24°$. Such differences are explained by preferred orientation effects, as observed by Gazzano et al. in XDR pattern of PHB films isothermally crystallized from the melt at various temperatures [24].

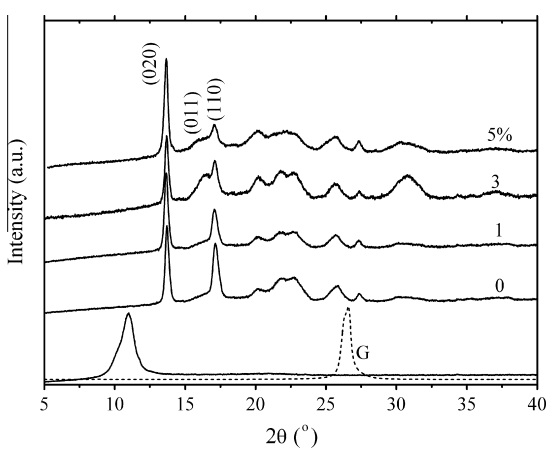

Fig. 1. X-ray diffraction patterns of graphite (G), graphite oxide, PHB, and nanocomposites containing 1, 3 and 5 wt% GO.

3.2. Thermal characterization

PHB is a natural product that is commercially available and can also be prepared at laboratory scale. Thermal decomposition temperatures (T_d) reported in the literature, however, vary widely typically between 250 °C and 285 °C. It is essential when modifying polyhydroxyalkanoates with additives, fillers or other polymer that the PHB constituent has a T_d as high as possible, close to 285 °C, which gives an indication of the purity of the PHB material under consideration.

The thermogravimetric traces of GO, PHB and the nanocomposites are shown in Fig. 2. The GO sample was prepared, similar to the nanocomposite films, by drop casting the dispersion in GBL onto a Teflon plate and drying at 130 °C for 16 h. As expected, the resulting GO thermogram was consistent with results published previously [20,23]. The thermogravimetric analysis of PHB and nanocomposites showed that T_d for pure PHB and nanocomposites remained unchanged up to 285 °C regardless of the amount of GO. The increasing weight loss observed around 200 °C was attributed to the increasing presence of GO in the nanocomposites. It is relevant to stress the importance of the acidic wash to the as-received PHB in order to properly assess the effect of GO on both the thermal and physical properties of PHB (see Section 2). The acidic wash is a key step for the fundamental study of PHB as it removes remaining metal ions from the as-received polymer. Metal ions are known to accelerate the polymer degradation process [25]. Thus, by treating as-received PHB with aqueous HCl, the T_d of PHB was observed to increase from 271 to 285 °C (Fig. 1 SI). Jing and Qiu have shown that by adding 1 and 2 wt% GO to a PHB, the T_d of their nanocomposites increased from 266 °C to 277 and 290 °C, respectively [26]. In the present study, a similar enhancement of T_d was also observed when incorporating 1 and 2 wt% of GO to the as-received PHB, namely, from 271 °C to 284 and 285 °C, respectively (Fig. 1 SI). However, the addition of GO had no effect on the T_d of PHB after purification using the aforementioned acidic wash. This may suggest that it is rather the interaction between GO and possible metal ions in the as-received PHB that caused the apparent

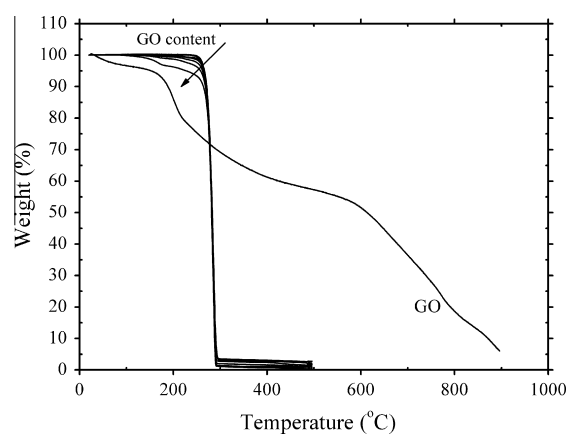

Fig. 2. TGA traces of GO, PHB, and nanocomposites containing 1–5 wt% GO at 10 °C min^{-1}.

increase of the T_d of the nanocomposites in the study by Jiu and Qiu.

3.3. Rheological characterization

Fig. 3 shows the dynamic shear modulus $|G^*(t_e)|$ of PHB and nanocomposites at 185 °C as a function of elapsed time (20 min "time sweep") in the linear viscoelastic region and measured at an angular frequency of 6.28 rad s^{-1}. For PHB, the shear modulus decreased with time due thermal degradation that takes place at 185 °C. Consequently, shorter polymer chains are randomly generated by the β-elimination mechanism which causes a molar mass reduction of the polymer while maintaining a constant PDI of 2 [27]. Decreasing molar mass of linear polymers generally results in a horizontal shift of the dynamic shear modulus–log frequency curve to higher frequencies. At constant frequency, as we performed our experiments, the dynamic shear modulus will then decrease and the phase angle δ increase towards 90°. The measurements are carried out at such temperature and frequency that the collected data cover the end of the rubber plateau including the terminal zone. By increasing the amount of GO in the polymer, the initial shear modulus of the nanocomposites was consistently enhanced, and the time dependence was reduced. The large changes in rheological properties with increasing GO content may reflect both micromechanical filler effects, which depend on filler volume fraction ϕ, moduli ratio, aspect ratio, and particle dispersion, as well as a possible influence of the GO particles on the thermal degradation of the PHB. From TGA measurements, often wrongly used as the sole measure of the thermal stability, no influence of GO on the decomposition temperature T_d was observed. However, molar mass determination before and after 20 min at 185 °C gave clear evidence for a degradation process with increasing degradation rate of PHB in the nanocomposites (Fig. 4). The sharp increase of the dynamic shear modulus shown in Fig. 3 can therefore be attributed to the micromechanical action of the nanoparticles, and can be further explored by evaluating the primary mea-

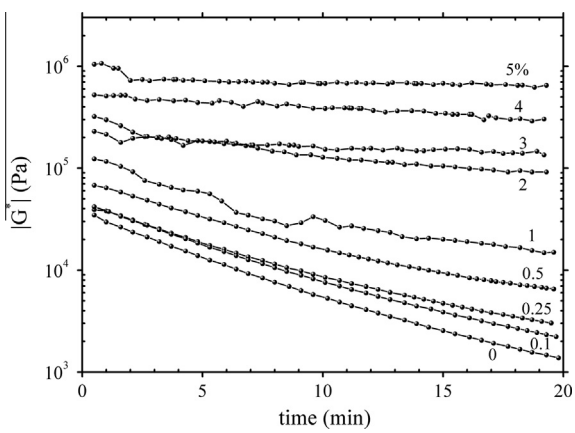

Fig. 3. Dynamic shear modulus $|G^*(t_e)|$ of PHB, and nanocomposites containing 0.1–5 wt% GO as a function of elapsed time at ω = 6.28 rad s^{-1} and 185 °C.

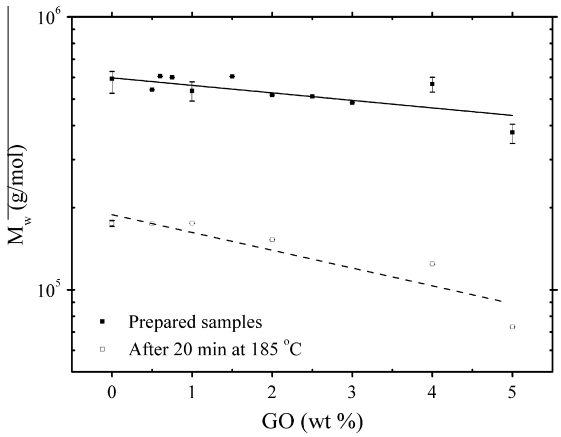

Fig. 4. Weight average molar mass (M_w) of PHB and nanocomposites as a function of added GO wt% for as-prepared samples [—], and for samples annealed at 185 °C for 20 min [–].

sured viscoelasctic quantities, the phase angle $\delta(t_e)$ and the dynamic shear modulus $|G^*(t_e)|$ as a function of elapsed time t_e at 185 °C and at angular frequency ω = 6.28 rad s^{-1}.

In Fig. 5, $\delta(t_e)$ vs $|G^*(t_e)|$ is plotted. This kind of plot has previously been very useful in exploring the structure and mobility of miscible and heterogeneous polymer blends [28–30]. Booij and Palmen [28] introduced the δ vs $|G^*|$ plot to determine a frequency and temperature independent apparent plateau modulus by extrapolating the phase angle δ to zero. Eklind and Maurer [29] used this type of plot extensively to characterize theoretically and experimentally the influence of morphology on the viscoelastic properties of heterogeneous polymer blends and discussed the advantages of the data analysis. Van Gurp and Palmen [30] used the δ vs $|G^*|$ plot to discuss time–temperature superposition of miscible and heterogeneous polymer blends. Other rheological data of viscoelastic polymer melts such as G' and G'', η' and η'', or η' and $|\eta^*|$ are derived from the primary data and contain in principle the same information. The use of the phase angle δ in this respect is advantageous as it allows an extrapolation to δ is zero. The apparent dynamic equilibrium modulus determined this way is independent of both frequency and molar mass. Two series of samples are prepared from two different solvent systems, namely, GBL and GBL/DMSO. The results are presented in Fig. 5a and b. The data in Fig. 5a and b are collected as a function of elapsed time t_e, and represent the effect of the continuously decreasing molar mass on the rheological data. Remarkably, for the sample series prepared with GBL (Fig. 5a), all the data in the terminal zone, including the non-filled PHB data, showed network formation and a GO-dependent equilibrium modulus by extrapolating

$$|G^*_{eq}| = \lim_{\delta \to 0^\circ} |G^*(t_e)| \quad (1)$$

On the other hand, for the series prepared with GBL/DMSO (Fig. 5b), network formation and equilibrium modulus dependence on GO was observed only for nanocomposites with concentrations equal or higher than 0.1 wt% of GO. Nevertheless, for both series, the network modulus

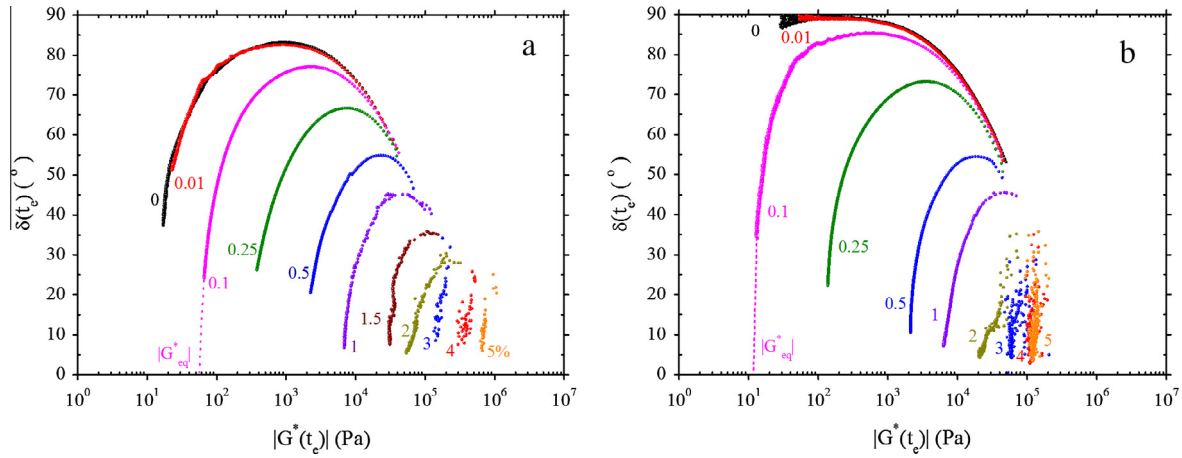

Fig. 5. Phase angle $\delta(t_e)$ vs the dynamic shear modulus $|G^*(t_e)|$for sample series prepared in (a) GBL and (b) GBL/DMSO, at $\omega = 6.28$ rad s^{-1}, and 185 °C. The equilibrium shear modulus $|G^*_{eq}|$ for 0.1 wt% GO, obtained by extrapolating $|G^*|$ as δ approaches 0°, are also indicated by the dotted line in both series.

strongly increased and scaled the GO volume fraction with $\phi^{2.42}$ as shown in Fig. 6. Therefore, although the existence of a weak structural network in unfilled PHB prepared with GBL remains unclear, the evidence showed that the effect of GO on the nanocomposites, hence the equal scaling behavior in both series, was independent of whether unfilled PHB included a weak network structure or not.

Shih et al. [31] developed a scaling theory using a fractal gel model, where the elastic shear modulus G' and the critical strain γ_c (limit of the linear viscoelastic region) of a colloidal gel both follow a power-law dependence of the volume fraction of the gel forming component. In the case where the links between the flocs had a higher elastic modulus than the links between particles, the theory predicts $G' \propto \phi^x$ and $\gamma_c \propto \phi^y$ where ϕ is the volume fraction of the filler, $x = (3 + b)/(3 - D)$, and $y = -(1 + b)/(3 - D)$. Here, D is the fractal dimension of the aggregate network, and b is an exponent that relates the particle volume fraction with aggregate size, being $1 < b < D$ [31]. Experimental values for the power-law exponent x for colloidal gels have been reported to lie between 2.4 and 4.4 [31–43]. In this study, Fig. 6 shows the relation $|G^*_{eq}| \propto \phi^{2.42}$, the power-law exponent of which $x = 2.42$ was found to be in line with aforementioned values. Furthermore, the limits of linearity of viscoelastic behavior were analyzed by performing "strain sweeps" at 6.28 rad s^{-1} and at 185 °C. Fig. 7 shows the dynamic shear modulus $|G^*(\gamma)|$ as a function of the strain amplitude for PHB and the nanocomposites (1–5 wt% GO), where critical strains γ_c are indicated. As predicted by the theory of Shih et al. [31], the limits of the linearity for PHB/GO nanocomposites followed a power-law dependence on the GO volume fraction, $\gamma_c \propto \phi^{-3.46}$ as shown in Fig. 8. Values reported in the literature for the power-law exponents for other heterogeneous materials, are also in line with the one obtained in this study [31–43]. Moreover, the abovementioned expressions describing the fractal aggregates model were determined to be $b = -7.7$ and $D = 4.9$. For the percolation of spherical particles to occur, and according to the scaling model, b must be

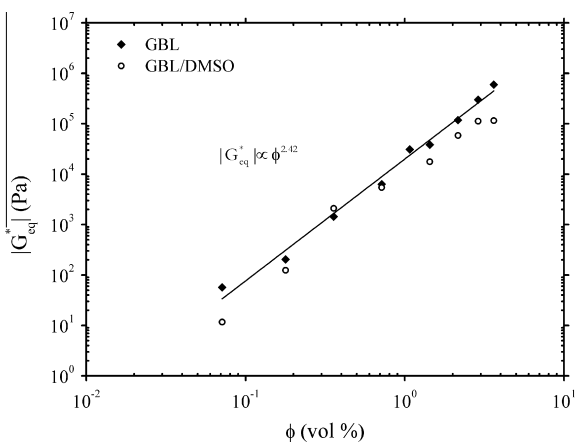

Fig. 6. Equilibrium shear modulus $|G^*_{eq}|$ of the sample series prepared in GBL [♦] and GBL/DMSO [○] as a function of GO volume fraction.

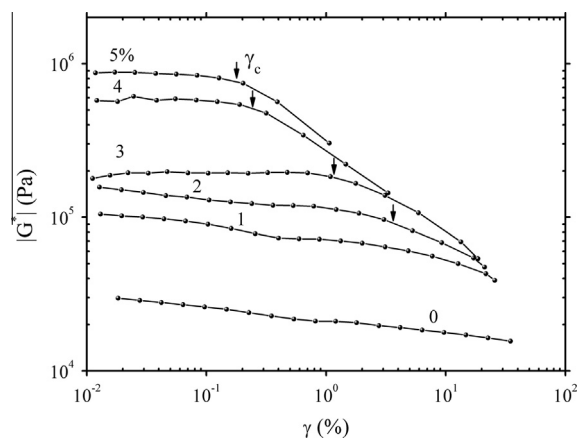

Fig. 7. Dynamic shear modulus $|G^*(\gamma)|$ of PHB, and nanocomposites containing 1–5 wt% GO as a function of strain amplitude γ at $\omega = 6.28$ rad s^{-1}, and 185 °C. The critical strain for the sample containing 1 wt% GO was not indicated since it could not be determined.

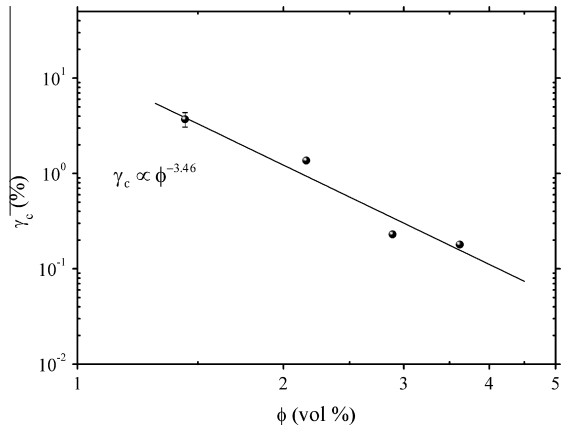

Fig. 8. Critical strain γ_c of the nanocomposites as a function of GO volume fraction.

larger than unity, which is not the case in this study. In addition, the other necessary condition for the theory to apply, $D < 3$, was not fulfilled either. This might indicate that the network formed in PHB/GO nanocomposites is not of fractal nature. Similar results were also obtained by Vermant et al. [38] for polypropylene/clay nanocomposites, where they concluded that the nature of the network was not fractal despite finding evidence for local aggregations.

According to Ren et al. [44], the relationship between the aspect ratio of the disk-shape nanofiller and the percolation volume fraction, assuming a randomly oriented and monodispersed system, is equal to:

$$\xi = \frac{3\phi_s}{2\phi_p} \tag{2}$$

where ξ is the aspect ratio, described as the ratio of width to thickness of the filler, $\phi_s = 0.29$ is the onset of percolation of interpenetrating, randomly packed spheres, and ϕ_p the percolation volume fraction. The percolation volume fraction, defined as the volume fraction at which a space-filling network of GO particles is first formed, was obtained at 0.1 wt% GO. This was the composite with the lowest loading where an equilibrium modulus was measured (Fig. 5b). This definition would not apply for the series prepared with GBL (Fig. 5a). However, also for this series it was at 0.1 wt% GO where the equilibrium modulus of the nanocomposite started to increase and scaled as $|G^*_{eq}| \propto \phi^{2.42}$. Using Equation (2) and $\phi_p = 7 \times 10^{-4}$ (0.1 wt% GO), an aspect ratio equal to 400 was determined. Furthermore, assuming the dimensions of the monolayer GO obtained by the Hummer's method to be on the order of 1 μm in lateral size, and between 0.7 and 1 nm in thickness [45–47], additional information of the dimension of GO sheets forming the network in the nanocomposites was estimated. By assuming that the network is mainly by single layers of GO, lateral sizes ranging from 280 to 400 nm can be deduced. On the other hand, if the lateral size of 1 μm is assumed a network composed of bi- or trilayer of GO sheets would be the case. In this study, the latter situation is considered more likely due to the tendency to re-stacking of the GO sheets.

3.4. Solid state characterization

Dynamic mechanical analyses in the terminal zone of the viscoelastic behavior of the melt are very sensitive to changes in molecular mobility of the matrix and network formation. However, in the solid state, these weak network forces play a minor role, and the structure and aspect ratio of the nanofiller, as well as the moduli of the constituents are dominant factors for the viscoelastic behavior of the nanocomposites. In the case of semi-crystalline polymers nanocomposites, the degree of crystallinity will in turn determine the modulus of the matrix. For this purpose, the effect of GO on the thermal properties of the nanocomposites was study by DSC (Figs. 2 and 3 SI). As it was observed, the addition of GO to PHB caused only minor changes in the enthalpy values of crystallization ΔH_c, which indicated that the degree of crystallinity, and so the modulus, of the PHB matrix in the nanocomposites is similar after the preparation of the samples.

Suitable models such as the Halpin–Tsai model can be used to fit experimental data with two fitting parameters: the modulus of the nanofiller and its aspect ratio ξ [48]. In the present study, the determination of shear moduli, instead of the E moduli, was preferred since they are only slightly dependent on the orientation distribution of anisotropic particles [49]. The expression for the Halpin–Tsai model for platelet reinforcement used was:

$$\frac{|G^*_{nano}|}{|G^*_{PHB}|} = \frac{1 + \xi\eta\phi}{1 - \eta\phi} \tag{3}$$

with:

$$\eta = \frac{|G^*_{GO}|/|G^*_{PHB}| - 1}{|G^*_{GO}|/|G^*_{PHB}| + \xi} \tag{4}$$

where $|G^*_{nano}|$, $|G^*_{PHB}|$, and $|G^*_{GO}|$ are the shear modulus of the nanocomposite, PHB, and GO, respectively, and ξ is the aspect ratio. Solid state dynamic shear measurements of PHB and the GO nanocomposites were performed at 30 °C in the linear viscoelastic region at constant strain amplitude of 0.2%, and an angular frequency of 62.83 rad s^{-1}. Fig. 9 represents the shear modulus of PHB and the nanocomposites as a function of GO volume fraction and aging time of 1, 5 and 25 days after preparation of the samples. All moduli increased with time probably due to secondary crystallization effects and physical aging effects. All data can be well described by Eq. (3), using the already determined aspect ratio of 400, and by fitting the shear modulus of GO to an average value of 17.5×10^9 Pa for the different aging times. This rather low value of the apparent shear modulus of GO, in comparison to expected single sheet properties, is comparable to the range of E moduli of 6–24 GPa reported for tiled GO layers in GO paper [50–53]. It is worth mentioning, however, that according to the modified Halpin–Tsai model in this study, the ratio $|G^*_{GO}|/|G^*_{PHB}|$ becomes almost independent of the aspect ratio for values higher than 100 (Fig. 4 SI).

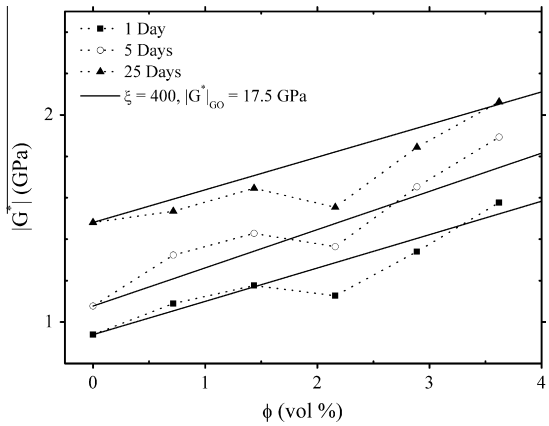

Fig. 9. Dynamic shear modulus of PHB and nanocomposites at $\omega = 62.8$ rad s^{-1}, and 30 °C. 1 [■], 5 [○], and 25 [▲] days after their preparation. The straight curves are fitted by the modified Halpin–Tsai model for an aspect ratio ξ of 400 and GO apparent shear modulus $|G^*|_{GO}$ of 17.5 GPa.

4. Conclusions

PHB nanocomposites based on GO were prepared by casting from GBL mixtures. Microstructural analysis of the nanocomposites revealed an efficient exfoliation of the GO, indicated by the absence of the reflection associated to the nanofiller in the XRD diffraction patterns. The decomposition temperature of PHB recorded by TGA remained unchanged with the incorporation of GO. However, molar mass measurements indicated that GO had a negative influence on the thermal stability of the polymer. Melt rheology was used to analyze and characterize the dispersion and network formation of GO nanoplatelets in the nanocomposites. The increase of the dynamic shear modulus of the nanocomposites was attributed to the micromechanical action and network formation of the GO nanoparticles. Analysis of the primary viscoelastic quantities, the phase angle $\delta(t_e)$ and the dynamic shear modulus $|G^*|(t_e)$, as well as the variation of the limits of linearity of viscoelastic behavior were used to evaluate the GO dependent network. Power-law dependencies of the equilibrium shear modulus $|G^*_{eq}|$ and the limits of linearity on GO volume fraction were found to fit well the experimental data, $|G^*_{eq}| \propto \phi^{2.42}$, and $\gamma_c \propto \phi^{-3.46}$. However, according to the scaling theory for colloidal gels as a collection of fractal aggregates, where both power-law scaling apply, the nature of the GO network could not be ascribed as such. Moreover, a corresponding aspect ratio ξ of GO was determined to be 400. Solid state dynamic shear measurements were analyzed according to the Halpin–Tsai model for platelet reinforcement, where the shear modulus of GO was used as the fitting parameter. Consequently, using the calculated aspect ratio, an average value for the GO apparent shear modulus of 17.5 GPa was determined, indicating a GO network structure including tiled GO layers.

Acknowledgements

We thank the Swedish Research Council for Environment, Agricultural Sciences and Spatial Planning (Formas) for the financial support, Annika Weiber from the Department of Chemistry, Polymer & Materials Chemistry at Lund University, and Alan Werker, Peter Johansson and Per Magnusson from AnoxKaldnes AB for valuable discussions.

Carola Müller from the Department of Chemistry, Polymer & Materials Chemistry, Lund University, for the powder XRD measurements.

Appendix A. Supplementary material

Supplementary data associated with this article can be found, in the online version, at http://dx.doi.org/10.1016/j.eurpolymj.2014.07.035.

References

[1] Dawes EA, Senior PJ. The role and regulation of energy reserve polymers in micro-organisms. In: Rose AH, Tempest DW, editors. Advances in microbial physiology. Academic Press; 1973. p. 135–266.
[2] Inoue Y, Yoshie N. Structure and physical-properties of bacterially synthesized polyesters. Prog Polym Sci 1992;17(4):571–610.
[3] Morikawa H, Marchessault RH. Pyrolysis of bacterial polyalkanoates. Can J Chem 1981;59(15):2306–13.
[4] Marchessault RH, Coulombe S, Morikawa H, Okamura K, Revol JF. Solid state properties of poly-β-hydroxybutyrate and of its oligomers. Can J Chem 1981;59(1):38–44.
[5] Ballistreri A, Garozzo D, Giuffrida M, Impallomeni G, Montaudo G. Analytical degradation – an approach to the structural-analysis of microbial polyesters by different methods. J Anal Appl Pyrolysis 1989;16(3):239–53.
[6] Okada A, Usuki A. Twenty years of polymer–clay nanocomposites. Macromol Mater Eng 2006;291(12):1449–76.
[7] Moniruzzaman M, Winey KI. Polymer nanocomposites containing carbon nanotubes. Macromolecules 2006;39(16):5194–205.
[8] Kim H, Abdala AA, Macosko CW. Graphene/polymer nanocomposites. Macromolecules 2010;43(16):6515–30.
[9] Kuila T, Bose S, Mishra AK, Khanra P, Kim NH, Lee JH. Chemical functionalization of graphene and its applications. Prog Mater Sci 2012;57(7):1061–105.
[10] Hummers WS, Offeman RE. Preparation of graphitic oxide. J Am Chem Soc 1958;80(6):1339.
[11] Yoon S, In I. Role of poly(N-vinyl-2-pyrrolidone) as stabilizer for dispersion of graphene via hydrophobic interaction. Mater Sci 2011;46(5):1316–21.
[12] Zhu Y, Stoller MD, Cai W, Velamakanni A, Piner RD, Chen D, et al. Exfoliation of graphite in propylene carbonate and thermal reduction of the resulting graphene oxide platelets. ACS Nano 2010;4(2):1227–33.
[13] Pan Y, Wu T, Bao H, Li L. Green fabrication of chitosan films reinforced with parallel aligned graphene oxide. Carbohydr Polym 2011;83(4):1908–15.
[14] Ramanathan T, Abdala AA, Stankovich S, Dikin DA, Herrera-Alonso M, Piner RD, et al. Functionalized graphene sheets for polymer nanocomposites. Nat Nanotechnol 2008;3(6):327–31.
[15] Kim H, Macosko CW. Morphology and properties of polyester/exfoliated graphite nanocomposites. Macromolecules 2008;41(9):3317–27.
[16] Raghu AV, Lee YR, Jeong HM, Shin CM. Preparation and physical properties of waterborne polyurethane/functionalized graphene sheet nanocomposites. Macromol Chem Phys 2008;209(24):2487–93.
[17] Song P, Cao Z, Cai Y, Zhao L, Fang Z, Fu S. Fabrication of exfoliated graphene-based polypropylene nanocomposites with enhanced mechanical and thermal properties. Polymer 2011;52(18):4001–10.
[18] Shim SH, Kim KT, Lee JU, Jo WH. Facile method to functionalize graphene oxide and its application to poly(ethylene terephthalate)/graphene composite. ACS Appl Mater Interfaces 2012;4(8):4184–91.
[19] Wan C, Chen B. Reinforcement of biodegradable poly(butylene succinate) with low loadings of graphene oxide. J Am Chem Soc 2013;127(6):5094–9.
[20] Dimiev A, Kosynkin DV, Alemany LB, Chaguine P, Tour JM. Pristine graphite oxide. J Am Chem Soc 2012;134(5):2815–22.

[21] Mermoux M, Chabre Y, Rousseau A. FTIR and 13C NMR study of graphite oxide. Carbon 1991;29(3):469–74.
[22] Szabó T, Berkesi O, Forgó P, Josepovits K, Sanakis Y, Petridis D, et al. Evolution of surface functional groups in a series of progressively oxidized graphite oxides. Chem Mater 2006;18(11):2740–9.
[23] Poh HL, Sanek F, Ambrosi A, Zhao G, Sofer Z, Pumera M. Graphenes prepared by Staudenmaier, Hofmann and Hummers methods with consequent thermal exfoliation exhibit very different electrochemical properties. Nanoscale 2012;4(11):3515–22.
[24] Gazzano M, Tomasi G, Scandola M. X-ray investigation on melt-crystallized bacterial poly(3-hydroxybutyrate). Macromol Chem Phys 1997;198(1):71–80.
[25] Csomorova K, Rychly J, Bakos D, Janigova I. The effect of inorganic additives on the decomposition of poly(beta-hydroxybutyrate) into volatile products. Polym Degrad Stab 1994;43(3):441–6.
[26] Jing X, Qiu Z. Crystallization kinetics and thermal property of biodegradable poly(3-hydroxybutyrate)/graphene oxide nanocomposites. Nanosci Nanotechnol 2012;12(9):7314–21.
[27] Martens AA, Besseling NAM, Rueb S, Sudhölter EJR, Spaink HP, de Smet LCPM. Random scission of polymers: numerical simulations, and experiments on hyaluronan hydrolysis. Macromolecules 2011;44(8):2559–67.
[28] Booij HC, MPalmen JH. Linear viscoelastic properties of melts of miscible blends of poly(methylmethacrylate) with poly(ethylene oxide). Theor Appl Rheol 1992:321.
[29] Eklind H, Maurer FHJ. On the morphology determination of heterogeneous blends by melt-state dynamic mechanical spectroscopy. Networks Blends 1995;5(1):35–45.
[30] Van Gurp M, Palmen J. Time–temperature superposition for polymeric blends. Rheol Bull 1998;67(1):5–8.
[31] Shih WH, Shih WY, Kim SI, Liu J, Aksay IA. Scaling behavior of the elastic properties of colloidal gels. Phys Rev A 1990;42(8):4772–9.
[32] Buscall R, McGowan IJ. Sedimentation and viscous flow of a weakly flocculated concentrated dispersion. A comparative study. Faraday Discuss 1983;76:277–90.
[33] Buscall R, McGowan IJ, Mumme-Young CA. Rheology of weakly interacting colloidal particles at high concentration. Faraday Discuss 1990;90:115–27.
[34] van der Aerschot E, Mewis J. Equilibrium properties of reversibly flocculated dispersions. Colloids Surf 1992;69(1):15–22.
[35] Bremer LGB, Bijsterbosch BH, Schrijvers R, van Vliet T, Walstra P. On the fractal nature of the structure of acid casein gels. Colloids Surf 1990;51:159–70.
[36] Durmus A, Kasgoz A, Macosko CW. Linear low density polyethylene (LLDPE)/clay nanocomposites. Part I: structural characterization and quantifying clay dispersion by melt rheology. Polymer 2007;48(15):4492–502.
[37] Kim H, Macosko CW. Processing–property relationships of polycarbonate/graphene composites. Polymer 2009;50(15):3797–809.
[38] Vermant J, Ceccia S, Dolgovskij MK, Maffettone PL, Macosko CW. Quantifying dispersion of layered nanocomposites via melt rheology. J Rheol 2007;51(3):429–50.
[39] Stauffer D, Coniglio A, Adam M. Gelation and critical phenomena. In: Dušek K, editor. Polymer networks. Berlin, Heidelberg: Springer; 1982. p. 103–58.
[40] Martin JE, Wilcoxon J, Adolf D. Critical exponents for the sol–gel transition. Phys Rev A 1987;36(4):1803–10.
[41] Takigawa T, Takahashi M, Urayama K, Masuda T. Comparison of model prediction with experiment for concentration-dependent modulus of poly(vinyl alcohol) (PVA) gels near the gelation point. Chem Phys Lett 1992;195(5–6):509–12.
[42] Sonntag RC, Russel WB. Structure and breakup of flocs subjected to fluid stresses. I. Shear experiments. J Colloid Interface Sci 1986;113(2):399–413.
[43] Buscall R, Mills PDA, Stewart RF, Sutton D, White LR, Yates GE. The rheology of strongly-flocculated suspensions. J Non-Newtonian Fluid Mech 1987;24(2):183–202.
[44] Ren J, Silva AS, Krishnamoorti R. Linear viscoelasticity of disordered polystyrene–polyisoprene block copolymer based layered-silicate nanocomposites. Macromolecules 2000;33(10):3739–46.
[45] Parades JI, Villar-Rodil S, Martínez-Alonso A, Tascón JMD. Graphene oxide dispersions in organic solvents. Langmuir 2008;24(19):10560–4.
[46] Park S, An J, Piner RD, Jung I, Yang D, Velamakanni A, et al. Aqueous suspension and characterization of chemically modified graphene sheets. Chem Mater 2008;20(21):6592–4.
[47] Dreyer DR, Park S, Bielawski CW, Ruoff RS. The chemistry of graphene oxide. Chem Soc Rev 2010;39(1):228–40.
[48] Van Es M. Ph.D. thesis, Delft University of Technology, Delft, The Netherlands; 2001.
[49] Nielsen LE. Mechanical properties of polymers and composites, vol. 2. New York: Marcel Dekker; 1974. p. 387.
[50] Dikin DA, Stankovich S, Zimney EJ, Piner RD, Dommett GHB, Evmenenko G, et al. Preparation and characterization of graphene oxide paper. Nature 2007;448(7152):457–60.
[51] Chen H, Müller MB, Gilmore KJ, Wallace GG, Li D. Mechanically strong, electrically conductive, and biocompatible graphene paper. Adv Mater 2008;20(18):3557–61.
[52] Chen C, Yang QH, Yang Y, Lv W, Wen Y, Hou PX, et al. Self-assembled free-standing graphite oxide membrane. Adv Mater 2009;21(29):3007–11.
[53] Imperiali L, Liao KH, Clasen C, Fransaer J, Macosko CW, Vermant J. Interfacial rheology and structure of tiled graphene oxide sheets. Langmuir 2012;28(21):7990–8000.